Salt adaptability in a halophytic soybean (Glycine soja) involves photosystems coordination

Kun Yan (kyan@yic.ac.cn)
Yantai Institute of Coastal Zone Research
Wenjun He
Yantai Institute of Coastal Zone Research
Lanxing Bian
Yantai Institute of Coastal Zone Research
Zishan Zhang
Shandong Agriculture University College of Life Sciences
Xiaoli Tang
Ludong University
Mengxin An
Ludong University
Lixia Li
Yantai University
Guangxuan Han
Yantai Institute of Coastal Zone Research

Research article

Keywords: chlorophyll fluorescence; chloroplast ultrastructure; modulated 820 nm reflection; oxidative stress; photoinhibition

Posted Date: December 18th, 2019

DOI: https://doi.org/10.21203/rs.2.14648/v2

Version of Record: A version of this preprint was published at BMC Plant Biology on April 10th, 2020. See the published version at https://doi.org/10.1186/s12870-020-02371-x.

Abstract

Background: Glycine soja is a halophytic soybean native to saline soil in Yellow River Delta, China. Photosystem I (PSI) performance and the interaction between photosystem II (PSII) and PSI remain unclear in Glycine soja under salt stress. This study aimed to explore salt adaptability in Glycine soja in terms of photosystems coordination. Results: Potted Glycine soja was exposed to 300 mM NaCl for 9 days with a cultivated soybean, Glycine max , as control. Under salt stress, the maximal photochemical efficiency of PSII (Fv/Fm) and PSI (△MR/MR 0) were significantly decreased with the loss of PSI and PSII reaction center proteins in Glycine max , and greater PSI vulnerability was suggested by earlier decrease in △MR/MR 0 than Fv/Fm and depressed PSI oxidation in modulated 820 nm reflection transients. Inversely, PSI stability was defined in Glycine soja , as △MR/MR 0 and PSI reaction center protein abundance were not affected by salt stress. Consistently, chloroplast ultrastructure and leaf lipid peroxidation were not affected in Glycine soja under salt stress. Inhibition on electron flow at PSII acceptor side helped protect PSI by restricting electron flow to PSI and seemed as a positive response in Glycine soja due to its rapid recovery after salt stress. Reciprocally, PSI stability aided in preventing PSII photoinhibition, as the simulated feedback inhibition by PSI inactivation induced great decrease in Fv/Fm under salt stress. In contrast, PSI inactivation elevated PSII excitation pressure through inhibition on PSII acceptor side and accelerated PSII photoinhibition in Glycine max , according to the positive and negative correlation of △MR/MR 0 with efficiency that an electron moves beyond primary quinone and PSII excitation pressure respectively. Conclusion: Therefore, photosystems coordination depending on PSI stability and rapid response of PSII acceptor side contributed to defending salt-induced oxidative stress on photosynthetic apparatus in Glycine soja . Photosystems interaction should be considered as one of the salt adaptable mechanisms in this halophytic soybean.

Background

It is a great challenge to supply increasing population with enough food in future under the background of worldwide land degradation [1, 2]. Soil salinization is a major kind of land degradation and poses a serious threat to sustainable agricultural production. Irrigated farmland usually confronts secondary salinization because of unreasonable irrigation and fertilization, whereas large areas of saline land due to primary salinization are distributed in coastal zone and inland arid region [1]. In contrast to single soil improvement, biosaline agriculture has been proposed as an environmental friendly approach for managing saline land [3-5]. Halophytic crops are important germplasm resource, and besides direct planting in saline land, they also can be used for breeding new genotypes with salt tolerance by traditional hybridization or gene transformation. However, it is better to ascertain physiological mechanisms for adapting to saline stress in halophytes beforehand.

Salt stress disturbs plant metabolisms and inhibits plant growth by inducing osmotic stress and ionic toxicity, and as a salt-induced secondary stress, oxidative damage on biological macromolecules often arises [6-8]. Correspondingly, plants have evolved some defensive mechanisms such as root Na^+ exclusion, osmolyte synthesis and antioxidant induction. These defensive mechanisms generally work

more effectively in halophytes, and additionally, some special defensive behaviors exist in halophytes for their survival in saline land, such as salt secretion by glands and salt accumulation in vacuoles as osmolytes [8-12]. Plant survival and growth largely depend on photosynthesis. Photosynthesis is very sensitive to salt stress, and photosynthetic capacity seems to be a feasible criterion for differentiating plant salt tolerance [13-18]. In general, stomatal limitation on photosynthesis initially occurs due to salt-induced osmotic stress, and the inhibition on dark enzymatic processes can further reduce CO_2 fixation [17, 19, 20]. As a consequence, excitation pressure in chloroplast may be elevated to induce photosystems photoinhibition with excess ROS production [21, 22]. At present, most studies focus on salt-induced photosystem II (PSII) photoinhibition, and halophytes generally have higher PSII photochemical capacity and CO_2 assimilation rate than the glycophytic relatives under salt stress [14, 23, 24]. However, it remains unclear whether PSII components involving reaction center, donor and acceptor electron carriers have the uniform response in halophyte under salt stress.

Up to now, very limited attention has been paid to photosystem I (PSI) under salt stress, let alone the interaction between PSII and PSI [16]. In our recent studies, PSI was proved to be a crucial photoinhibition site in some glycophytic crops under salt stress [18, 25, 26]. Unlike PSII, it is hard to repair damaged PSI [22]. PSI photoinhibition can intensify PSII excitation pressure through feedback inhibition on electron transport and aggravate PSII photoinhibition [27, 28]. Accordingly, PSI inactivation has been found in susceptible plant species or cultivars with weak adaptability to abiotic stresses [18, 25, 28]. In contrast, PSII photoinhibition which restricts electron donation to PSI can help to prevent PSI photoinhibition by reducing ROS generation through Mehler reaction at PSI acceptor side [29-33]. Therefore, PSII and PSI coordination plays an important role in protecting the whole photosynthetic apparatus. In addition to great ability to defense ionic toxicity and osmotic stress, halophytes can effectively dissipate excitation energy in chloroplast and scavenge ROS for protecting PSII from oxidative damage, and PSII photoinhbition is rarely reported in halophytes under salt stress [14, 23, 24, 34]. Notably, PSII stability can elevate the possibility of PSI oxidative injury in halophytes particularly under long-term severe salt stress with tremendous decrease in CO_2 assimilation. Up to now, PSII and PSI coordination has not been reported in halophytes upon salt stress, and it remains unknown whether halophytes can protect PSI against photoinhibition by the flexible response of PSII.

Wild soybeans are precious germplasm resources for improving environmental adaptability in cultivated soybean. *Glycine cyrtoloba* is a wild soybean species native to saline soil in Australian beach, and a series of studies have demonstrated its high salt tolerance in terms of inhibiting Na^+ accumulation, photosynthetic activity, antioxidant activity, cyclic electron flow around PSI and excitation energy dissipation [23, 34-36]. In China, a halophytic soybean, *Glycine soja*, grows in coastal saline land in Yellow River Delta, and similar to *Glycine cyrtoloba*, *Glycine soja* also can effectively retard toxic ions accumulation and maintain high photosynthetic activity under salt stress [24, 37, 38]. In a recent study, we systematically illustrated salt tolerance in *Glycine soja* from the aspects of root ions flux, antioxidant system, osmotic regulation and photosynthesis [14]. Nonetheless, photosynthetic analysis was mainly concentrated on gas exchange characterization in these halophytic soybeans upon salt stress, and PSII

salt tolerance was only defined by no obvious change in the maximal photochemical efficiency of PSII (Fv/Fm). Fv/Fm cannot reflect heterogeneous behaviors of PSII components [39], and PSI performance and the coordination between PSII and PSI remain unclear in the halophytic soybean under salt stress. In this study, we attached importance to photosystem performance and photosynthetic electron transport, and aimed to deeply reveal salt adaptability in *Glycine soja* by elucidating photosystems coordination. This study can provide an insight to crop salt tolerance and may assist in soybean germplasm improvement.

Results

Gas exchange, electron transport rate and PSII excitation pressure

Photosynthetic rate (Pn), stomatal conductance (g_s) and PSII electron transport rate (ETR) were significantly decreased in the leaves of *Glycine soja* and *Glycine max* under salt stress, and greater decrease was noted in *Glycine max* (Fig. 1abd). Under salt stress, PSII excitation pressure (1-qP) was significantly increased by 35.6% in *Glycine max* at day 3, and the increase reached 72.5% at day 9 (Fig. 1c). After 6 days of salt stress, significant increase in 1-qP was observed in *Glycine soja*, and the increase was up to 50.3% at day 9 (Fig. 1c).

Prompt chlorophyll *a* fluorescence (PF), delayed chlorophyll *a* fluorescence (DF) and modulated 820 nm reflection transients (MR)

J step suggests kinetic bottlenecks of electron transport chain due to momentary maximum accumulation of reduced primary quinone (Q_A), and I step occurs due to the limitation of plastoquinone (PQ) re-oxidation [40, 41]. After 3 days of salt stress, J and I steps were obviously elevated in *Glycine max* (Fig. 2a), and the elevation of J and I steps became greater upon salt stress for 9 days (Fig. 2b), suggesting that PQ re-oxidation and electron transfer at PSII side beyond Q_A were inhibited. K step usually arises around 300 μs due to the injury on OEC at PSII donor side [42, 43]. After 3 days of salt stress, PSII donor side was impaired in *Glycine max* according to the appearance of K step (Fig. 2a). Comparatively, salt stress induced smaller elevation of J and I steps with no change in K step in *Glycine soja* (Fig. 2ab).

MR signals are presented by MR/MR_0 ratio, where MR_0 is the value at onset of actinic illumination (at 0.7 ms). PSI oxidation was initiated with the decrease in MR/MR_0 from MR_0 to the minimal value (MRmin) in MR transient, and subsequently, the increase of MR/MR_0 to the maximal level (MRmax) indicates PSI re-reduction. MR transient remarkably changed with significantly decreased MR_0-MRmin and MRmax-MRmin in *Glycine max* under salt stress (Fig. 2cd), suggesting that both PSI oxidation and re-reduction were negatively affected. In contrast, PSI oxidation and re-reduction were not inhibited by salt stress in *Glycine soja*, as no obvious change was found in MR_0-MRmin, MRmax-MRmin and MR transient (Fig. 2cd). Under salt stress, DF transient in *G. max* was prominently depressed with significant decrease in I_1 and I_2 peaks, but I_1 and I_2 peaks were slightly declined in *Glycine soja* (Fig. 2ef).

Immunoblot analysis, PSII performance and the maximal photochemical capacity of PSI

After 9 days of salt stress, PSI reaction center protein (PsaA) and PSII reaction center protein (PsbA) abundance were obviously declined in *Glycine max* rather than *Glycine soja* (Fig. 3ab). Total performance index (PI_{total}), PSII performance index (PI_{abs}), efficiency that an electron moves beyond Q_A (ETo/TRo) and probability with which an electron from the intersystem electron carriers is transferred to reduce end electron acceptors at the PSI acceptor side (REo/ETo) were significantly declined by salt stress in *Glycine max* and *Glycine soja*, and the decrease was greater in *Glycine max* (Fig. 3cdij). Significant decrease in the maximal photochemical capacity of PSI ($\triangle MR/MR_0$) was noted in *Glycine max* rather than *Glycine soja* under salt stress, and salt-induced decrease in Q_A reducing reaction centers per PSII antenna chlorophyll (RC/ABS) was also observed in *Glycine max* (Fig. 3fg). In line with elevated K step (Fig. 2ab), salt-induced significant increase in variable fluorescence intensity at K step (V_k) was also found in *Glycine max* (Fig. 3h). When salt stress was prolonged to 9 days, Fv/Fm was significantly decreased in *Glycine max*, but the decrease in Fv/Fm was not significant in *Glycine soja* (Fig. 3e).

Recovery of photosystem performance

One day after the cease of salt stress, PI_{total}, PI_{abs}, ETo/TRo and REo/ETo in salt-treated *Glycine soja* rapidly recovered to the normal level in *Glycine soja* without salt treatment, implying the high salt tolerance of photosystems in *Glycine soja* (Table 1). Probably due to irreversible damage on photosystems, these parameters did not show recovery in *Glycine max* despite the cease of salt stress (Table 1).

The coordination between PSI and PSII

$\triangle MR/MR_0$ was significantly and positively correlated with ETo/TRo in *Glycine max* under salt stress, while significant and negative correlation was noted between $\triangle MR/MR_0$ and 1-qP (Fig. 4ac). However, there was very low correlation of $\triangle MR/MR_0$ with ETo/TRo and 1-qP in *Glycine soja* (Fig. 4ac). The application of DCMU, an inhibitor blocking the electron transport from Q_A^- to Q_B^-, caused much greater decrease in Fv/Fm and ETo/TRo in *Glycine max* and *Glycine soja* after 9 days of salt stress (Fig. 4bd).

Fv/Fm with presence of chloramphenicol

Chloramphenicol, an inhibitor of D1 protein de novo synthesis, was used to clarify whether the difference of D1 protein de novo synthesis was responsible for unequal PSII photoinhibition in *Glycine max* and *Glycine soja*. Due to the application of chloramphenicol, Fv/Fm was greater decreased to a similar level in *Glycine max* and *Glycine soja* upon salt stress (Fig. 5), suggesting that the negative effects of salt stress was imposed on PSII mainly by impeding D1 protein repair.

Lipid peroxidation and H_2O_2 content

Malondialdehyde (MDA) content reflects the level of lipid peroxidation in plant tissue. After 9 days of salt stress, MDA and H_2O_2 content was significantly increased in the leaves of *Glycine max* in contrast to no remarkable change in the leaves of *Glycine soja*, and consistently, histochemical staining with 3,3-diaminobenzidine also suggested the obvious increase of H_2O_2 content in the leaves of *Glycine max* rather than *Glycine soja* (Fig. 6).

Ultrastructure of leaf chloroplast

After 9 days of salt stress, no obvious change occurred in mesophyll cell and chloroplast ultrastructure in *Glycine soja*, illustrating its high salt tolerance (Fig. 7). Nonetheless, chloroplast tended to separate from cell wall with great reduction of starch granules in *Glycine max* upon salt stress, and in addition to disintegrated chloroplast envelope, distended and loosen thylakoids were also detected (Fig. 7). The damage on chloroplast ultrastructure was accordant with salt-induced great depression on photosystems performance in *Glycine max*.

Discussion

As with our previous study [14], tremendous decrease in Pn with stomatal closure was verified in *Glycine max* and *Glycine soja* under severe salt stress (Fig. 1ab). The great depression on CO_2 assimilation posed a big threat to photosynthetic apparatus by increasing the possibility of ROS generation through feedback inhibition on photosynthetic electron transport. Actually, elevated lipid peroxidation and H_2O_2 concentration confirmed salt-induced oxidative stress in the leaves of *Glycine max* (Fig. 6). Photosystems photoinhibition usually arises in parallel with elevated leaf lipid peroxidation under environmental stresses, and notably, the negative correlation of ROS production with PSI and PSII photochemical capacity under salt stress has been evidenced [18, 25, 28, 44]. As a result, unchanged lipid peroxidation and H_2O_2 concentration implied that photosystems were less endangered by salt-induced oxidative stress in *Glycine soja* than *Glycine max*.

Consistently, salt-induced PSII and PSI photoinhibition was noted in *Glycine max* rather than *Glycine soja* according to the variation of Fv/Fm and $\triangle MR/MR_0$, and less decrease in PI_{total} corroborated better performance of photosynthetic apparatus in *Glycine soja* (Fig. 3cef). In particular, salt-induced destruction of chloroplast and thylakoid ultrastructure confirmed the serious depression on photosystems performance in *Glycine max* (Fig. 7). PSI vulnerability usually lies in sensitive plants and seems as a feasible criterion for discerning plant tolerance to abiotic stresses because of its threat to the entire photosynthetic apparatus [28]. In this study, PSI stability was defined in *Glycine soja* under salt stress due to unobvious change in $\triangle MR/MR_0$ and PsaA abundance (Fig. 3af). In contrast, PSI vulnerability was observed in *Glycine max*, indicated by salt-induced decrease in $\triangle MR/MR_0$ at day 3 before the occurrence of PSII photoinhibition (Fig. 3ef). Therefore, high salt adaptability should include PSI stability in the halophytic soybean. PI_{abs} comprehensively reflects PSII performance and is more sensitive than Fv/Fm [45, 46]. After 3 days of salt stress, PSII performance was already depressed not only in *Glycine max* but

also in *Glycine soja*, and less decease in PI_{abs} suggested greater PSII stability in *Glycine soja* (Fig. 3d). Under salt stress, PSII donor and acceptor sides were initially impaired with declined amount of active PSII reaction centers in *Glycine max* (Fig. 3gij), and PSII reaction center was damaged later due to lowered Fv/Fm and PsbA abundance (Fig. 3be). Comparatively, only PSII acceptor side was influenced by salt stress in *Glycine soja*, and the influence was lighter than that in *Glycine max* in light of less decrease in ETo/TRo and smaller elevation of J step (Fig. 2ab, 3i). Similar to previous study, PSII stability was verified in the halophytic soybean under salt stress [14, 24], however, the rapid response from PSII acceptor side was revealed in this study. Delayed chlorophyll *a* fluorescence in microsecond domain is mostly related to $Z^+Q_A^-$ state of PS II [47]. The occurrence of I_1 peak in DF transients mainly results from accumulation of $S_3Z^+P680Q_A^-$ state, which relates to active reaction centers and electron transfer capacity at both donor and acceptor sides of PSII [47, 48]. Under salt stress, large decrease in I_1 corroborated the damage on PSII components including reaction center, donor and acceptor sides in *Glycine max*, whereas slight decrease in I_1 was coincident with the mild inhibition on electron transport at PSII acceptor side in *Glycine soja* (Fig. 2ef). Overall, PSI stability and rapid response of PSII acceptor side were illustrated in the halophytic soybean under salt stress.

As reported in previous studies, antioxidant enzymes were stimulated by salt stress to a higher level in *Glycine soja* than *Glycine max* [14]. Apart from the stronger antioxidant protection, photosystems coordination also played an important role in counteracting photosystems photoinhibtion in *Glycine soja* exposed to severe salt stress. PSI photoinhibition derives from oxidation of iron-sulfur protein by ROS generated through Mehler reaction at PSI acceptor side, and the electron flow from PSII is essential for PSI photoinhibition [22]. Upon salt-induced great decrease in CO_2 assimilation, the rapid response of PSII acceptor side restricted electron flow to PSI in *Glycine soja* and could help protect against PSI inhibition by reducing ROS generation (Fig. 1d). The experiment with DCMU application, which simulated the suppression of electron transport at PSII acceptor side caused by PSI photoinhibition, demonstrated that PSI photoinhibition accelerated PSII photoinhibition (Fig. 4bd). PSI activity bore no relation to PSII excitation pressure and electron transport at PSII acceptor side in *Glycine soja* according to the correlation analysis of $\triangle MR/MR_0$ with 1-qP and ETo/TRo (Fig. 4ac). Therefore, PSI stability was conductive to preventing the occurrence of PSII photoinhibition by alleviating feedback inhibition on electron transport in *Glycine soja* under salt stress. Inversely, PSI vulnerability elevated PSII excitation pressure in *Glycine max* under salt stress by inducing over-reduction of PSII acceptor side, indicated by positive correlation between $\triangle MR/MR_0$ and ETo/TRo and negative correlation between $\triangle MR/MR_0$ and 1-qP (Fig. 1c, 4ac), and eventually resulted in PSII photoinhibition (Fig. 3e). The difference of salt-induced PSII photoinhibition between *Glycine max* and *Glycine soja* originated from the repair of photodamaged PSII rather than direct photodamage to PSII, because Fv/Fm decreased to the same level in presence of chloramphenicol (Fig. 5). The declined PSI re-reduction amplitude in MR transients conformed to PSII inactivation in *Glycine max* (Fig. 2cd), as PSI re-reduction process mainly depended on electron donation from PSII. In spite of great restriction on electron flow to PSI due to PSII inactivation, PSI oxidation amplitude in MR transient was still depressed (Fig. 2cd), which verified greater damage on PSI than PSII.

I_2 phase in DF transients is related to the prolonged reopening of PSII reaction centers by electron transfer from reduced quinone to plastoquinone (PQ) before full reduction of PQ pool [43, 44, 49]. In agreement with elevated I step and decreased REo/ETo, the decrease in I_2 also suggested that PQ re-oxidation was inhibited due to greater damage on PSI (Fig. 2ef). Therefore, the passive PSII photoinhibition could not effectively defend oxidative injury of PSI in *Glycine max* under salt stress. Nonetheless, salt stress also elevated I step and induced decrease in REo/ETo and I_2 in *Glycine soja* (Fig. 2abef, 3j), and the declined PQ re-oxidation seemed contradictory to unchanged PSI activity. PQ is located in cytochrome b6f complex (cyt b6f) by which electron transport from PSII to PSI is bridged, and the soluble primary PSI acceptor, Ferredoxin, binds the stromal site of cyt b6f to trigger PSI cyclic electron flow [50]. PSI cyclic electron flow is an important photoprotective pathway in plants under abiotic stress due to the reduction of electron donation to PSI and production of ATP for repairing photodamaged PSII [51-54]. We supposed that the declined PQ re-oxidation resulted from enhanced binding of cyt b6f with Fd for promoting PSI cyclic electron flow in *Glycine soja* under salt stress and caused feedback inhibition on electron transport beyond Q_A at PSII acceptor side. This inference should be established in future study by exploring the relation between photosystem coordination and PSI cyclic electron flow. However, at least, rapid recovery of ETo/TRo and REo/ETo after salt stress supported that it was a positive response to limit electron transport between PSII and PSI in *Glycine soja* for protecting photosynthetic apparatus (Table 1).

Conclusion

To summarize, photosystems coordination which was dependent on PSI stability and rapid response of PSII acceptor side contributed to defending salt-induced oxidative stress on photosynthetic apparatus in *Glycine soja*. This study can deepen the knowledge about salt tolerance mechanism in the halophyte.

Methods

Plant material and treatment

Glycine soja is a halophytic soybean native to coastal saline soil in Yellow River Delta, China. The seeds of *Glycine soja* were carefully collected from wild plants, identified by Prof. Hualing Xu and deposited in Dongying academy of agricultural sciences. Experimental research on plants including collection of plant material in this study did not violate any guideline or local legislation. Special permissions and ethical approval were not required to collect and use this wild soybean. *Glycine max* is a widely planted soybean cultivar in China, and the seeds of *Glycine max* were obtained from Shandong academy of agricultural sciences. The seeds of *Glycine soja* and *Glycine max* are shown in Additional file 1: Figure S1, and the seed specimens were, respectively, conserved in Dongying academy of agricultural sciences and Shandong academy of agricultural sciences without voucher number.

The protocols for seed germination and seedling culture have been reported in our previous study [14]. In July 7, 2017, the seeds of *Glycine max* were fully soaked in distilled water for 8 h, while the seeds of *Glycine soja* were soaked in concentrated sulfuric acid for 10 min to remove the hard shell over the seeds.

Then, the seeds were placed in petri dishes in the dark between two sheets of filter paper at 25 °C to germinate, and the filter paper was kept wet by spraying Hoagland nutrient solution (pH 5.7). Thereafter, the seedlings were transferred to plastic pots filled with vermiculite, watered with Hoagland solution (pH 5.7) and grown in artificial climatic chambers (Huier, China). The photon flux density, day/night temperature and humidity were controlled at 200 mmol m^{-2} s^{-1} (12 h per day from 07:00 to 19:00), 25/18 ^{o}C and 65% in the chamber. One month later, uniform plants were selected for salt treatment. NaCl was added to Hoagland nutrient solution (pH, 5.7) incrementally by 50 mM step every day to provide final concentration of 300 mM, and thereafter, salt stress (300 mM NaCl) persisted for 9 days. The newest fully expanded leaves were sampled for measuring physiological and biochemical parameters. After 9 days of salt stress, NaCl in the culture medium were leached completely with Hoagland nutrient solution for examining the recovery of photosystem performance.

Measurements of gas exchange and modulated chlorophyll fluorescence

Gas exchange and modulated chlorophyll fluorescence parameters were simultaneously detected by using an open photosynthetic system (LI-6400XTR, Li-Cor, Lincoln, NE, USA) equipped with a fluorescence leaf chamber (6400-40 LCF, Li-Cor). The temperature and CO_2 concentration were respectively set at 25 ^{o}C and 400 μmol mol^{-1} in the leaf cuvette. Pn and g_s were simultaneously recorded. Steady-state fluorescence yield was also recorded, and then a saturating actinic light pulse of 8000 μmol m^{-2} s^{-1} for 0.7 s was used to produce maximum fluorescence yield by temporarily inhibiting PSII photochemistry for measuring actual photochemical efficiency of PSII (ΦPSII). ETR was calculated as ΦPSII×PPFD×0.84×0.5 [55], and photochemical quenching coefficient was noted for calculating 1-qP.

Measurements of prompt chlorophyll fluorescence, delayed chlorophyll fluorescence and modulated 820 nm reflection transients

The measurements were conducted by using a multifunctional plant efficiency analyzer (MPEA, Hansatech, UK). The leaves were adapted in dark for 30 min, and thereafter, the leaves were illuminated with 1 s red light (627 nm, 5000 μmol photons m^{-2} s^{-1}) and subsequently with 10 s far red light (735 nm, 200 μmol photons m^{-2} s^{-1}). PF, DF and MR transients were simultaneously recorded in the first 1 s illumination with red light, and MR signals were still detected in the following 10 s far red illumination. The redox state of PSI reaction center under continuous light can be detected by monitoring 820 nm reflection [40]. $\Delta MR/MR_0$ was calculated according to the relative difference of 820 nm reflection between the maximal oxidized and reduced PSI reaction center [40, 56]. PF transients were quantified by JIP test to calculate Fv/Fm, V_k, RC/ABS, ETo/TRo, REo/ETo, PI_{abs} and PI_{total} [57].

All redox reactions of the photosynthetic electron transport are reversible, and the back electron transfer and charge recombination in PSII reaction center lead to delayed fluorescence emission from repopulated excited chlorophyll [47]. DF signals are recorded in dark intervals for excluding PF interference under the light [47, 57]. In this study, DF signals in microsecond domain were collected at 20 μs after turning off actinic light for constructing DF transients.

Measurements of MDA and H_2O_2 contents and histochemical detection of H_2O_2

MDA content was measured by thiobarbituric acid reaction method for indicating lipid peroxidation degree [58]. Leaf tissues (0.5 g) were ground under liquid nitrogen and homogenized in 5 mL 0.1% TCA. The homogenate was centrifuged at 10000 × *g* and 4 °C for 10 min to collect the supernatant for measuring MDA and H_2O_2 contents [25]. Leaves were vacuum-infiltrated with 0.1 mg ml^{-1} 3, 3-diaminobenzidine in 50mM tris-acetate solution (pH, 3.8) and incubated at room temperature in the dark for 24 h. Thereafter, the leaves were decolorized by immersion in boiling ethanol (80%) for 10 min and photographed [59].

Isolation of thylakoid membranes and western blot

As with the method of Yan et al. [28], thylakoid membrane proteins were extracted from the leaves, separated by a 12% (w/w) SDS-PAGE gel and transferred onto polyvinylidene fluoride membranes. After blocking with 5% skimmed milk for 1h, the membranes were incubated with primary anti-PsbA and anti-PsaA antibodies respectively and then incubated with horseradish peroxidase-conjugated anti-rabbit IgG antibody (PhytoAB, USA). The BeyoECL Plus substrate (Beyotime Biotechnology, China) was applied to test immunoreaction, and the chemiluminescence was recorded by using a Tanon-5500 cooled CCD camera (Tanon, China).

Observation of chloroplast ultrastructure

Similar to Oustric et al. [60] with small modification, leaf pieces (1 mm^2) were sampled, fixed in 2.5 % glutaraldehyde in 100 mM phosphate buffer (pH, 7.2) for 2 h at room temperature and washed with the same buffer. The samples were post-fixed in 1 % osmic acid in 100 mM phosphate buffer (pH, 7.2) at room temperature for 4 h, parched through a graded ethanol series (50–100%) and embedded in Spurr's epoxy resin. Ultra-sections (70 nm) were prepared by using an ultramicrotome (Leica ultracut R, Germany) and stained with uranyl acetate and lead phosphate. A transmission electron microscope (JEM-1230, Japan) was used for observing chloroplast ultrastructure.

Statistical analysis

One-way ANOVA was carried out by using SPSS 16.0 (SPSS Inc., Chicago, IL, USA) for all sets of data. The values presented are the means of measurements with five replicate plants, and comparisons of means were determined through LSD test. Difference was considered significant at $P < 0.05$.

Abbreviations

Cyt b6f, cytochrome b6f complex; ETo/TRo, probability that an electron moves further than primary acceptor of PSII; ETR, PSII electron transport rate; Fv/Fm, the maximal quantum yield of PSII; g_s, stomatal conductance; MDA, malondialdehyde; Pn, photosynthetic rate; PI_{abs}, PSII performance index, PI_{total}, total performance index; PSI, Photosystem I; PSII, Photosystem II; RC/ABS, primary quinone reducing reaction

centers per PSII antenna chlorophyll; PQ, plastoquinone; REo/ETo, probability with which an electron from the intersystem electron carriers is transferred to reduce end electron acceptors at the PSI acceptor side; Q_A, primary quinone; ROS, reactive oxygen species; V_k, variable fluorescence intensity at K step; $\triangle MR/MR_0$, the maximal photochemical capacity of PSI; ΦPSII, actual photochemical efficiency of PSII; 1-qP, excitation pressure of PSII

Declarations

Ethics approval and consent to participate

Not applicable

Consent for publication

Not applicable

Availability of data and materials

All data generated or analyzed during this study are included in this published article.

Competing interests

The authors declare that they have no competing interests.

Funding

This research was jointly financed by Shandong Provincial Natural Science Foundation, China (ZR2017QC005), National Natural Science Foundation of China (41201292), Key Deployment Project of Chinese Academy of Sciences (KFZD-SW-112), Opening Foundation of the State Key Laboratory of Crop Biology, Shandong Agricultural University (2016KF07) and Shandong Key Research and Development Plan (2017CXGC0316). The funders were not involved in the experiment design, data collection and analysis, preparation of the manuscript, and decision to publish.

Authors' contributions

KY designed the experiment, performed the experiment and data analysis, wrote and revised the manuscript. WH and LB participated in the experiment. ZZ participated in the experiment and helped revise the manuscript. XT and MA participated in data analysis. LL helped polish the language. GH proposed some critical suggestions and reviewed the manuscript. All authors have read the manuscript and approved the final version of the manuscript.

Acknowledgements

We thank Prof. Hualing Xu for identifying the *Glycine soja* seeds.

References

1. Nikalje GC, Srivastava AK, Pandey GK, Suprasanna P. Halophytes in biosaline agriculture: Mechanism, utilization, and value addition. Land Degrad. Dev. 2017;29: 1081-1095.
2. Fedoroff NV, Battisti DS, Beachy RN, Cooper PJM, Fischhoff DA, Hodges CN, Knauf VC, Lobell D, Mazur BJ, Molden D, Reynolds MP, Ronald PC, Rosegrant MW, Sanchez PA, Vonshak A, Zhu JK. Radically rethinking agriculture for the 21st century. Science 2010;327: 833-834.
3. Panta S, Flowers T, Lane P, Doyle R, Haros G, Shabala S. Halophyte agriculture: Success stories. Environ. Exp. Bot. 2014;107: 71-83.
4. Rozema J, Flowers T. Ecology crops for a salinized world. Science. 2008;322: 1478-1480.
5. Ventura Y, Eshel A, Pasternak D, Sagi M. The development of halophyte-based agriculture: Past and present. Ann. Bot. 2015;115: 529-540.
6. Gill SS, Tuteja N. Reactive oxygen species and antioxidant machinery in abiotic stress tolerance in crop plants. Plant Physiol. Biochem. 2010;48: 909-930.
7. Hossain M.S, Dietz K.J. Tuning of redox regulatory mechanisms, reactive oxygen species and redox homeostasis under salinity stress. Front. Plant Sci. 2016;7: 548.
8. Bose J, Moreno AR, Shabala S. ROS homeostasis in halophytes in the context of salinity stress tolerance. J. Exp. Bot. 2014;65: 1241-1257.
9. Chen M, Yang Z, Liu J, Zhu T, Wei X, Fan H, Wang B. Adaptation mechanism of salt excluders under saline conditions and its applications. Int. J. Mol. Sci. 2018;19: 3668.
10. Shabala S, Bose J, Hedrich R. Salt bladders: Do they matter? Trends Plant Sci. 2014;19: 687-691.
11. Song J, Wang B. Using euhalophytes to understand salt tolerance and to develop saline agriculture: *Suaeda salsa* as a promising model. Ann. Bot. 2015;115: 541-553.
12. Wu H. Plant salt tolerance and Na^+ sensing and transport. Crop J. 2018; 6: 215-225.
13. Aparicio C, Urrestarazu M, Cordovilla MD. Comparative physiological analysis of salinity effects in six olive genotypes. Hortscience. 2014;49: 901-904.
14. Chen P, Yan K, Shao H, Zhao S. Physiological mechanisms for high salt tolerance in wild soybean (*Glycine soja*) from yellow river delta, China: Photosynthesis, osmotic regulation, ion flux and antioxidant capacity. PLoS One. 2013;8: e83227.
15. Kalaji HM, Govindjee, Bosa K, Koscielniak J, Golaszewska KZ. Effects of salt stress on photosystem II efficiency and CO_2 assimilation of two Syrian barley landraces. Environ. Exp. Bot. 2011;73: 64-72.
16. Stepien P, Johnson GN. Contrasting responses of photosynthesis to salt stress in the glycophyte arabidopsis and the halophyte Thellungiella: Role of the plastid terminal oxidase as an alternative electron sink. Plant Physiol. 2009;149: 1154-1165.
17. Yan K, Shao HB, Shao CY, Chen P, Zhao SJ, Brestic M, Chen XB. Physiological adaptive mechanisms of plants grown in saline soil and implications for sustainable saline agriculture in coastal zone. Acta Physiol. Plant. 2013;35: 2867-2878.

18. Yan K, Wu C, Zhang L, Chen X. Contrasting photosynthesis and photoinhibition in tetraploid and its autodiploid honeysuckle (*Lonicera japonica* thunb.) under salt stress. Front Plant Sci. 2015;6: 227.
19. Loreto F, Centritto M, Chartzoulakis K. Photosynthetic limitations in olive cultivars with different sensitivity to salt stress. Plant Cell Environ. 2003;26: 595-601.
20. Yang XH, Liang Z, Wen XG, Lu CM. Genetic engineering of the biosynthesis of glycinebetaine leads to increased tolerance of photosynthesis to salt stress in transgenic tobacco plants. Plant Mol. Biol. 2008;66: 73-86.
21. Takahashi S, Murata N. How do environmental stresses accelerate photoinhibition? Trends Plant Sci. 2008;13: 178-182.
22. Sonoike K. Photoinhibition of photosystem I. Physiol. Plant. 2011;142: 56-64.
23. Yang Y, Yan CQ, Cao BH, Xu HX, Chen JP, Jiang DA. Some photosynthetic responses to salinity resistance are transferred into the somatic hybrid descendants from the wild soybean *Glycine cyrtoloba* ACC547. Physiol. Plant. 2007;129: 658-669.
24. Xue Z, Zhao S, Gao H, Sun S. The salt resistance of wild soybean (*Glycine soja* Sieb. et Zucc. ZYD 03262) under NaCl stress is mainly determined by Na^+ distribution in the plant. Acta Physiol. Plant. 2013;36: 61-70.
25. Yan K, Bian T, He W, Han G, Lv M, Guo M, Lu M. Root abscisic acid contributes to defending photoinibition in Jerusalem artichoke (*Helianthus tuberosus* L.) under salt stress. Int J Mol Sci. 2018;19.
26. Yan K, Zhao S, Liu Z, Chen X. Salt pretreatment alleviated salt-induced photoinhibition in sweet sorghum. Theor. Exp. Plant Physiol. 2015;27: 119-129.
27. Zhang ZS, Yang C, Gao HY, Zhang LT, Fan XL, Liu MJ. The higher sensitivity of PSI to ROS results in lower chilling-light tolerance of photosystems in young leaves of cucumber. J. Photochem. Photobiol. B-Biol. 2014;137: 127-134.
28. Yan K, Zhao S, Cui M, Han G, Wen P. Vulnerability of photosynthesis and photosystem I in Jerusalem artichoke (*Helianthus tuberosus* L.) exposed to waterlogging. Plant Physiol. Biochem. 2018;125: 239-246.
29. Yan K, Chen P, Shao HB, Shao CY, Zhao SJ, Brestic M. Dissection of photosynthetic electron transport process in sweet sorghum under heat stress. PLoS One. 2013;8: e62100.
30. Yan K, Chen P, Shao HB, Zhao SJ. Characterization of photosynthetic electron transport chain in bioenergy crop Jerusalem artichoke (*Helianthus tuberosus* L.) under heat stress for sustainable cultivation. Ind. Crop. Prod. 2013;50: 809-815.
31. Zivcak M, Brestic M, Kalaji HM, Govindjee. Photosynthetic responses of sun- and shade-grown barley leaves to high light: Is the lower PSII connectivity in shade leaves associated with protection against excess of light? Photosynth. Res. 2014;119: 339-354.
32. Zhang ZS, Jia YJ, Gao HY, Zhang LT, Li HD, Meng QW. Characterization of PSI recovery after chilling-induced photoinhibition in cucumber (*Cucumis sativus* L.) leaves. Planta 2011;234: 883-889.

33. Zhang ZS, Jin LQ, Li YT, Tikkanen M, Li QM, Ai XZ, Gao HY. Ultraviolet-B radiation (UV-B) relieves chilling-light-induced PSI photoinhibition and accelerates the recovery of CO_2 assimilation in cucumber (*Cucumis sativus* L.) leaves. Sci Rep. 2016;6: 34455.
34. Lu KX, Ding WN, Zhu SH, Jiang DA. Salt-induced difference between *Glycine cyrtoloba* and *G. max* in anti-oxidative ability and K^+ vs. Na^+ selective accumulation. Crop J. 2016;4: 129-138.
35. Lu KX, Yang Y, He Y, Jiang DA. Induction of cyclic electron flow around photosystem I and state transition are correlated with salt tolerance in soybean. Photosynthetica. 2008;46: 10-16.
36. Yang Y, Jiang DA, Xu HX, Yan CQ, Hao SR. Cyclic electron flow around photosystem I is required for adaptation to salt stress in wild soybean species *Glycine cyrtoloba* ACC547. Biol. Plant. 2006;50: 586-590.
37. Wei P, Che B, Shen L, Cui Y, Wu S, Cheng C, Liu F, Li MW, Yu B, Lam HM. Identification and functional characterization of the chloride channel gene, *GsCLC-c2* from wild soybean. BMC Plant Biol. 2019; 19: 121.
38. Zhang XK, Zhou QH, Cao JH, Yu BJ. Differential Cl-/Salt Tolerance and NaCl-induced alternations of tissue and cellular ion fluxes in *Glycine max*, *Glycine soja* and their hybrid seedlings. J. Agron. Crop Sci. 2011;197: 329-339.
39. Li PM, Cheng LL, Gao HY, Jiang CD, Peng T. Heterogeneous behavior of PSII in soybean (*Glycine max*) leaves with identical PSII photochemistry efficiency under different high temperature treatments. J. Plant Physiol. 2009;166: 1607-1615.
40. Schansker G, Srivastava A, Govindjee, Strasser RJ. Characterization of the 820-nm transmission signal paralleling the chlorophyll a fluorescence rise (OJIP) in pea leaves. Funct. Plant Biol. 2003;30: 785-796.
41. Schansker G, Toth SZ, Strasser RJ. Methylviologen and dibromothymoquinone treatments of pea leaves reveal the role of photosystem I in the Chl a fluorescence rise OJIP. Biochim. Biophys. Acta. 2005;1706: 250-261.
42. Oukarroum A, Madidi SE, Strasser RJ. Differential heat sensitivity index in barley cultivars (*Hordeum vulgare* L.) monitored by chlorophyll a fluorescence OKJIP. Plant Physiol. Biochem. 2016;105: 102-108.
43. Oukarroum A, Goltsev V, Strasser RJ. Temperature effects on Pea plants probed by simultaneous measurements of the kinetics of prompt fluorescence, delayed fluorescence and modulated 820 nm reflection, PLoS One. 2013;8: 10.
44. Oukarroum A, Bussotti F, Goltsev V, Kalaji HM. Correlation between reactive oxygen species production and photochemistry of photosystems I and II in *Lemna gibba* L. plants under salt stress. Environ. Exp. Bot. 2015;109: 80-88.
45. Zivcak M, Brestic M, Olsovska K, Slamka P. Performance index as a sensitive indicator of water stress in *Triticum aestivum* L. Plant Soil Environ. 2008;54: 133-139.
46. Zivcak M, Olsovska K, Slamka P, Galambosova J, Rataj V, Shao HS, Brestic M. Application of chlorophyll fluorescence performance indices to assess the wheat photosynthetic functions

influenced by nitrogen deficiency. Plant Soil Environ. 2014;60: 210-215.

47. Goltsev V, Zaharieva I, Chernev P, Strasser RJ. Delayed fluorescence in photosynthesis. Photosynth. Res. 2009;101: 217-232.
48. Gao J, Li P, Ma F, Goltsev V. Photosynthetic performance during leaf expansion in *Malus micromalus* probed by chlorophyll a fluorescence and modulated 820nm reflection. J. Photochem. Photobiol. B-Biol. 2014;137: 144-150.
49. Kalaji HM, Goltsev V, Bosa K, Allakhverdiev SI, Strasser RJ, Govindjee. Experimental in vivo measurements of light emission in plants: A perspective dedicated to david walker. Photosynth. Res. 2012;114: 69-96.
50. Joliot P, Joliot A. Cyclic electron flow in C3 plants. Biochim. Biophys. Acta. 2006;1757: 362-368.
51. Wu X, Shu S, Wang Y, Yuan R, Guo S. Exogenous putrescine alleviates photoinhibition caused by salt stress through cooperation with cyclic electron flow in cucumber. Photosynth. Res. Online 2019.
52. Sun Y, Geng Q, Du Y, Yang X, Zhai H. Induction of cyclic electron flow around photosystem I during heat stress in grape leaves. Plant Sci. 2017;256: 65-71.
53. Huang W, Yang YJ, Zhang SB, Liu T. Cyclic electron flow around photosystem I promotes ATP synthesis possibly helping the rapid repair of photodamaged photosystem II at low light. Front. Plant Sci. 2018;9: 239.
54. Yang XQ, Zhang QS, Zhang D, Feng JX, Zhao W, Liu Z, Tan Y. Interaction of high seawater temperature and light intensity on photosynthetic electron transport of eelgrass (*Zostera marina* L.). Plant Physiol. Biochem. 2018;132: 453-464.
55. Maxwell K, Johnson GN. Chlorophyll fluorescence - a practical guide. J. Exp. Bot. 2000;51: 659-668.
56. Yan K, Han G, Ren C, Zhao S, Wu X, Bian T. Fusarium solani infection depressed photosystem performance by inducing foliage wilting in apple seedlings. Front. Plant Sci. 2018;9: 479.
57. Strasser RJ, Michael MT, Qiang S, Goltsev V. Simultaneous in vivo recording of prompt and delayed fluorescence and 820 nm reflection changes during drying and after rehydration of the resurrection plant haberlea rhodopensis. Biochim. Biophys. Acta. 2010;1797: 122.
58. Yan K, Zhao S, Bian L, Chen X. Saline stress enhanced accumulation of leaf phenolics in honeysuckle (*Lonicera japonica* thunb.) without induction of oxidative stress. Plant Physiol. Biochem. 2017;112: 326-334.
59. ThordalChristensen H, Zhang ZG, Wei YD, Collinge DB. Subcellular localization of H_2O_2 in plants. H_2O_2 accumulation in papillae and hypersensitive response during the barley-powdery mildew interaction. Plant J. 1997;11: 1187-1194.
60. Oustric J, Quilichini Y, Morillon R, Herbette S, Luro F, Giannettini J, Berti L, Santini J. Tetraploid citrus seedlings subjected to long-term nutrient deficiency are less affected at the ultrastructural, physiological and biochemical levels than diploid ones. Plant Physiol. Biochem. 2019;135: 372-384.

Table 1

Table 1. Recovery of Total performance index (PI_{total}), PSII performance index (PI_{abs}), efficiency that an electron moves beyond primary quinone (ETo/TRo,) and probability with which an electron from the intersystem electron carriers is transferred to reduce end electron acceptors at the PSI acceptor side (REo/ETo) for one day in the leaves of *Glycine soja* (GS) and *Glycine max* (GM) after 9 days of salt stress with 300 mM NaCl. Data in the table indicate the mean of five replicates (±SD). Within each row, means followed by the same letters are not significantly different between salt treatment and control at $P < 0.05$.

Parameters	GM	GM + NaCl	GS	GS + NaCl
PI_{total}	1.82±0.33a	0.58±0.21b	2.11±0.19a	2.03±0.13a
PI_{abs}	2.64±0.48a	0.78±0.12b	2.87±0.58a	2.69±0.41a
ETo/TRo	0.54±0.02a	0.43±0.03b	0.56±0.02a	0.54±0.04a
REo/ETo	0.41±0.03a	0.32±0.01b	0.42±0.03a	0.41±0.01a

Additional File Legend

Additional file 1: Figure S1 *Glycine soja* and *Glycine max* seeds, transients of prompt chlorophyll *a* fluorescence in *Glycine soja* and *Glycine max* before salt treatment, and the growth of *Glycine soja* and *Glycine max* in an artificial climatic chamber.

Figures

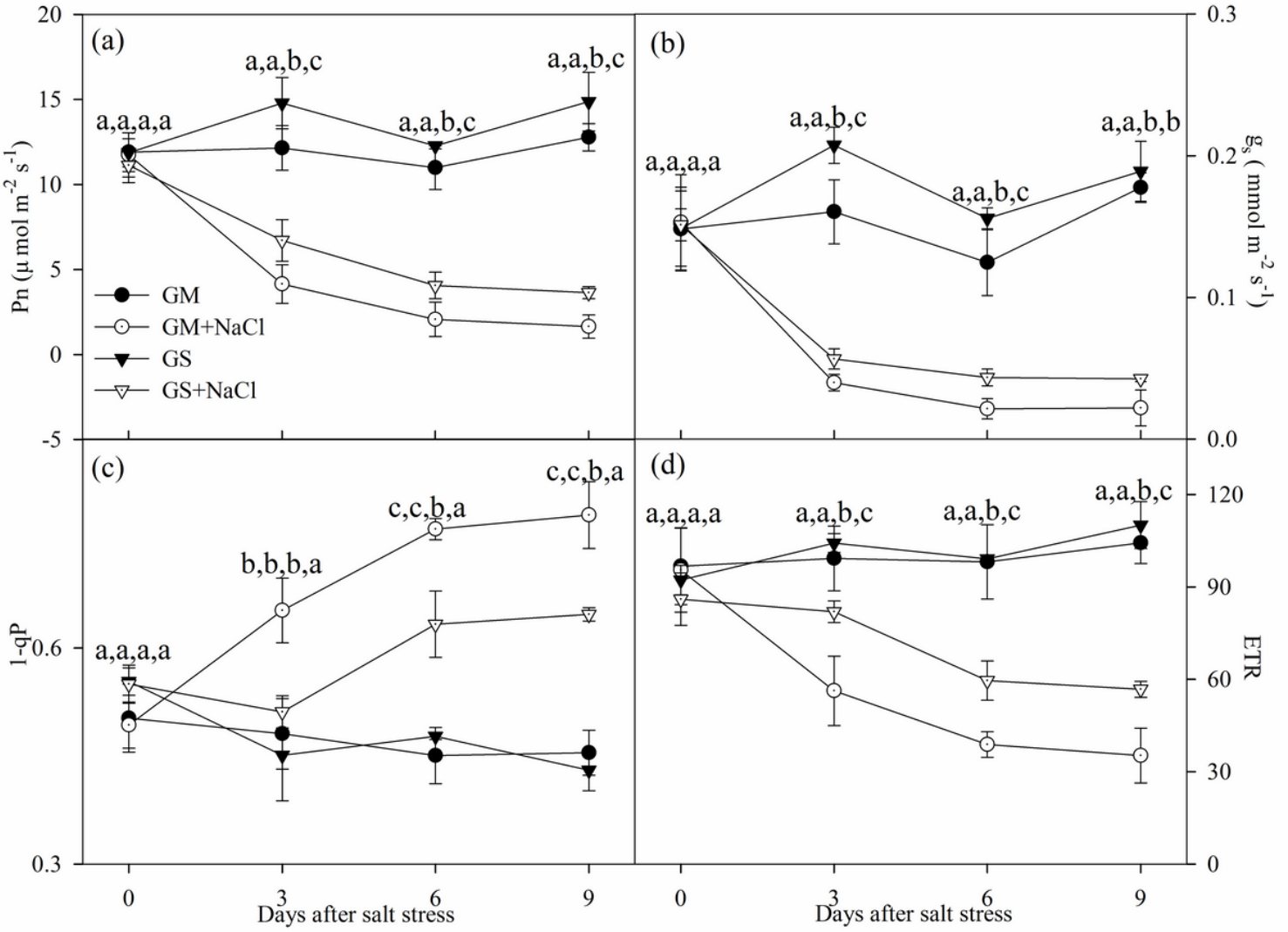

Figure 1

Photosynthetic rate (Pn, a), stomatal conductance (gs, b), PSII excitation pressure (1-qP, c) and PSII electron transport rate (ETR, d) in Glycine max (GM, circles) and Glycine soja (GS, triangles) exposed to 0 (closed symbols) and 300 mM (open symbols) NaCl. Data in the figure indicate the mean of five replicates (±SD). Different letters indicate significant difference among GS, GM, GS+NaCl and GM+NaCl at $P < 0.05$.

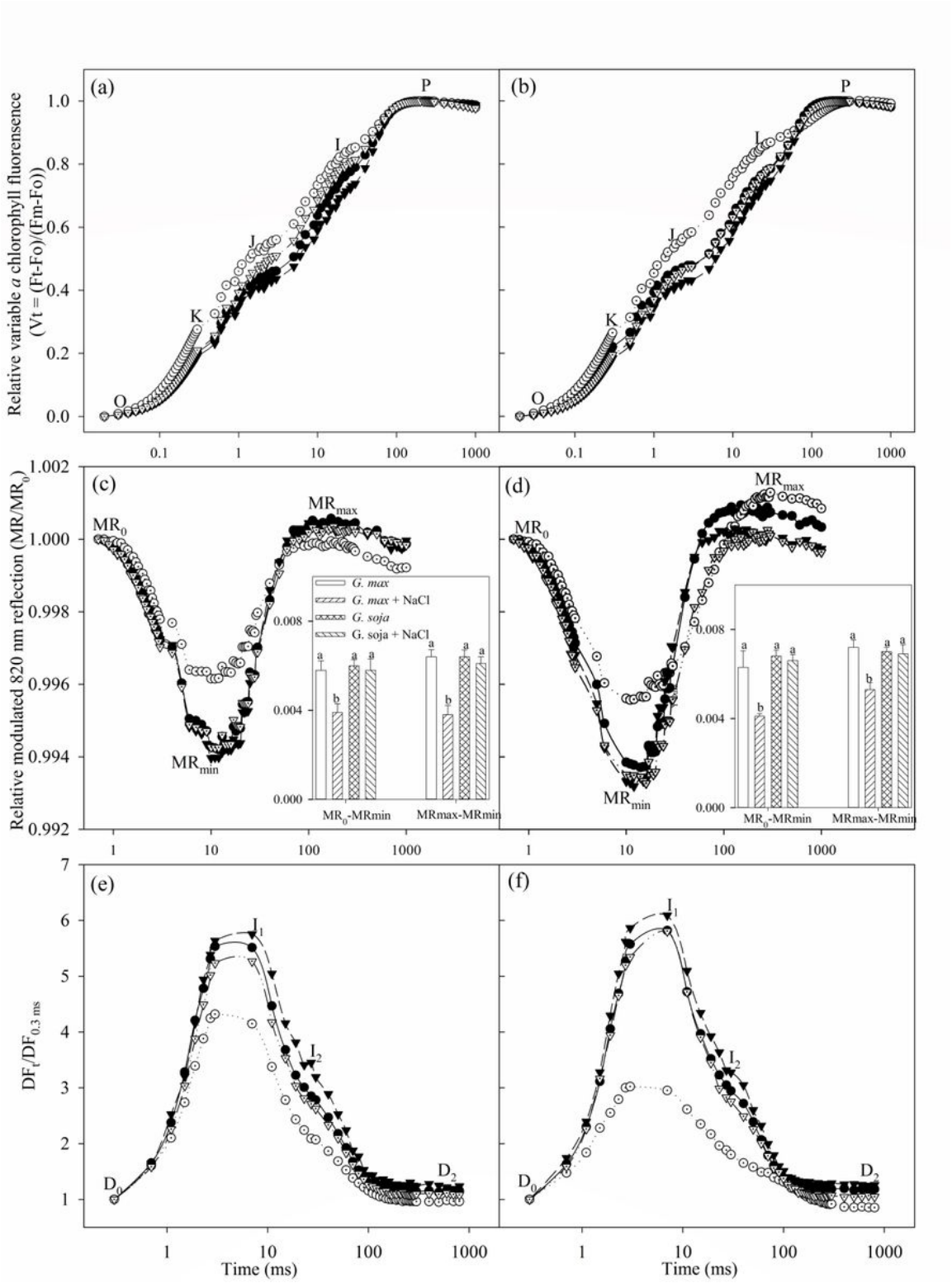

Figure 2

Transients of prompt chlorophyll a fluorescence (a, b), modulated 820 nm reflection (c, d), and delayed chlorophyll a fluorescence (e, f) in Glycine max (circles) and Glycine soja (triangles) exposed to 0 (closed symbols) and 300 mM (open symbols) NaCl for 3 (left panels) and 9 (right panels) days. O, K, J, I and P indicate the specific steps in chlorophyll a fluorescence transient. MR0 is the value of modulated 820 nm reflection at the onset of red light illumination (0.7 ms, the first reliable MR measurement). MR0-MRmin

and MRmax-MRmin were PSI oxidation and re-reduction amplitude, respectively. The data of MR0-MRmin and MRmax-MRmin indicate mean of five replicates (±SD), and different letters on error bars indicate significant difference at P < 0.05. Do, I1, I2, D2 indicate initial point, the first (7 ms) and second (50 ms) maximal peaks and minimum point in delayed chlorophyll a fluorescence curves. DF0.3ms is the initial microsecond delayed fluorescence signal at 0.3 ms. The signals were plotted on a logarithmic time scale, and each curve is the average of five replicates.

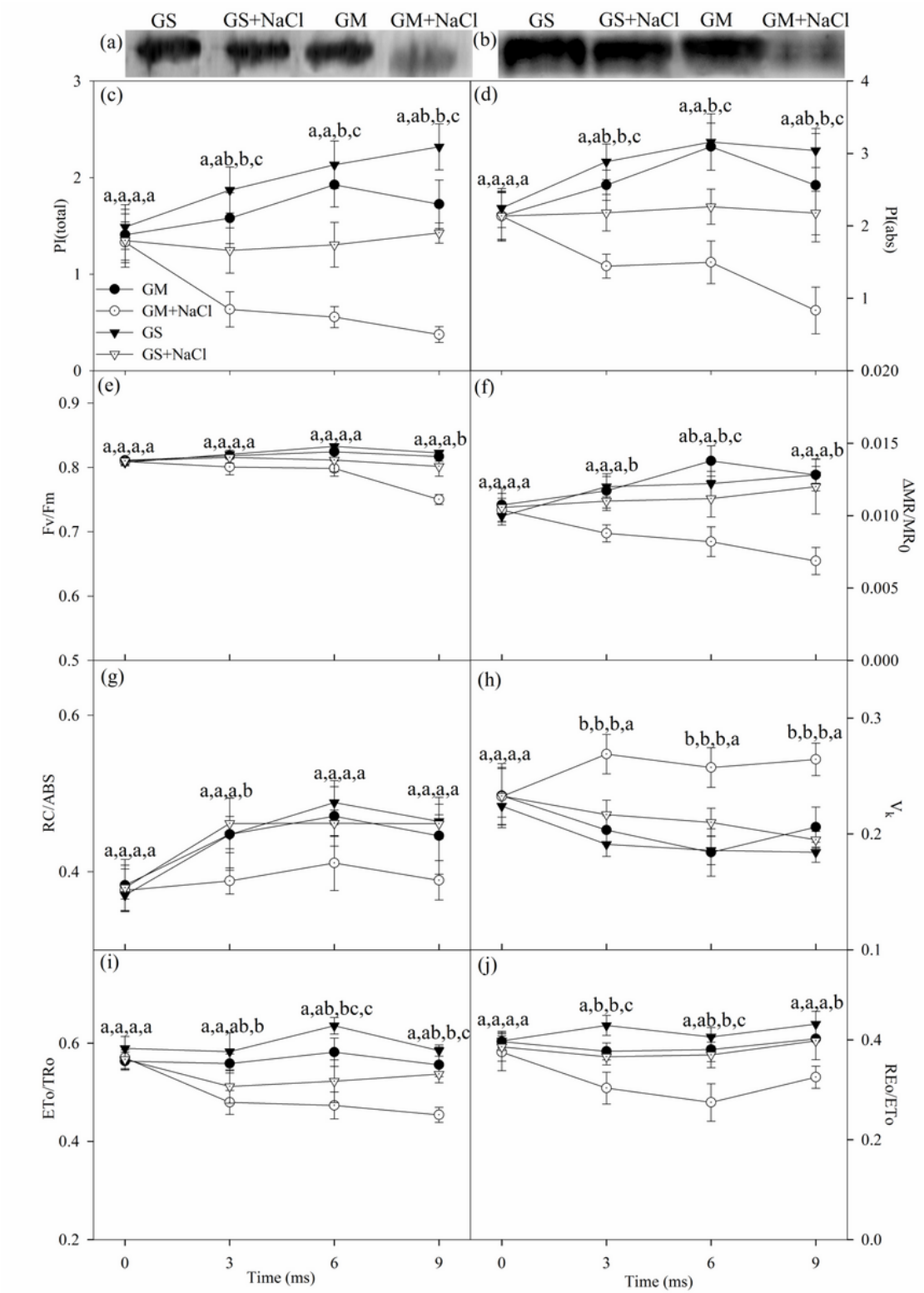

Figure 3

Immunoblot analysis of reaction center proteins of PSI (PsaA, a) and PSII (PsbA, b) in the leaves of Glycine max (GM) and Glycine soja (GS) after 9 days of salt stress with 300 mM NaCl. Total performance index (PItotal, c), PSII performance index (PIabs, d), the maximal photochemical efficiency of PSII (Fv/Fm, e) and PSI (△MR/MR0, f), primary quinone reducing reaction centers per PSII antenna chlorophyll (RC/ABS, g), variable fluorescence intensity at K step (Vk, h), efficiency that an electron moves beyond primary quinone (ETo/TRo, i) and probability with which an electron from the intersystem electron carriers is transferred to reduce end electron acceptors at the PSI acceptor side (REo/ETo, j) in the leaves of Glycine max (circles) and Glycine soja (triangles) exposed to 0 (closed symbols) and 300 mM (open symbols) NaCl. Data in the figure indicate the mean of five replicates (±SD). Different letters indicate significant difference among GS, GM, GS+NaCl and GM+NaCl at $P < 0.05$.

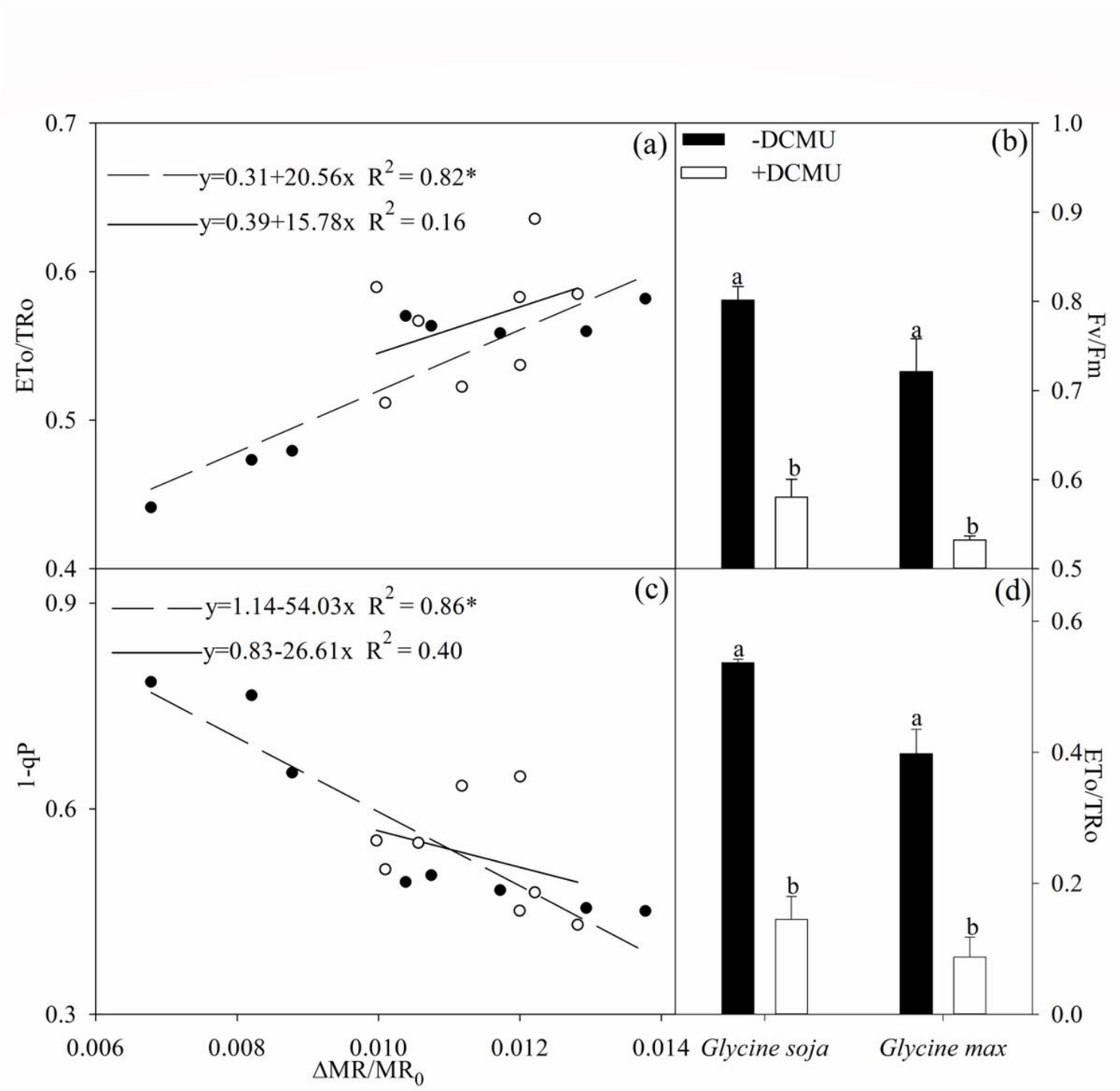

Figure 4

Regression analysis of the maximal photochemical efficiency of PSII (△MR/MR0) with probability that an electron moves further than primary quinone (ETo/TRo, a) and PSII excitation pressure (1-qP, c) in Glycine max (closed symbols) and Glycine soja (open symbols). * Indicates that the correlation was significant at P < 0.01. The maximal photochemical efficiency of PSII (Fv/Fm, b) and ETo/TRo (d) in Glycine max and Glycine soja in the absence or presence of 3-(3,4-dichlorfenyl)-1,1-dimethylkarbonyldi-amid (DCMU) after 9 days of salt stress with 300 mM NaCl. For reagent treatment, the leaves after 6 days of salt stress with 300 mM NaCl were immersed in 0 or 70 μM DCMU for 3 h in the dark. The data of

Fv/Fm (b) and ETo/TRo (d) indicate the mean of five replicates (±SD), and different letters on error bars indicate significant difference between DCMU treatment and control at P < 0.05.

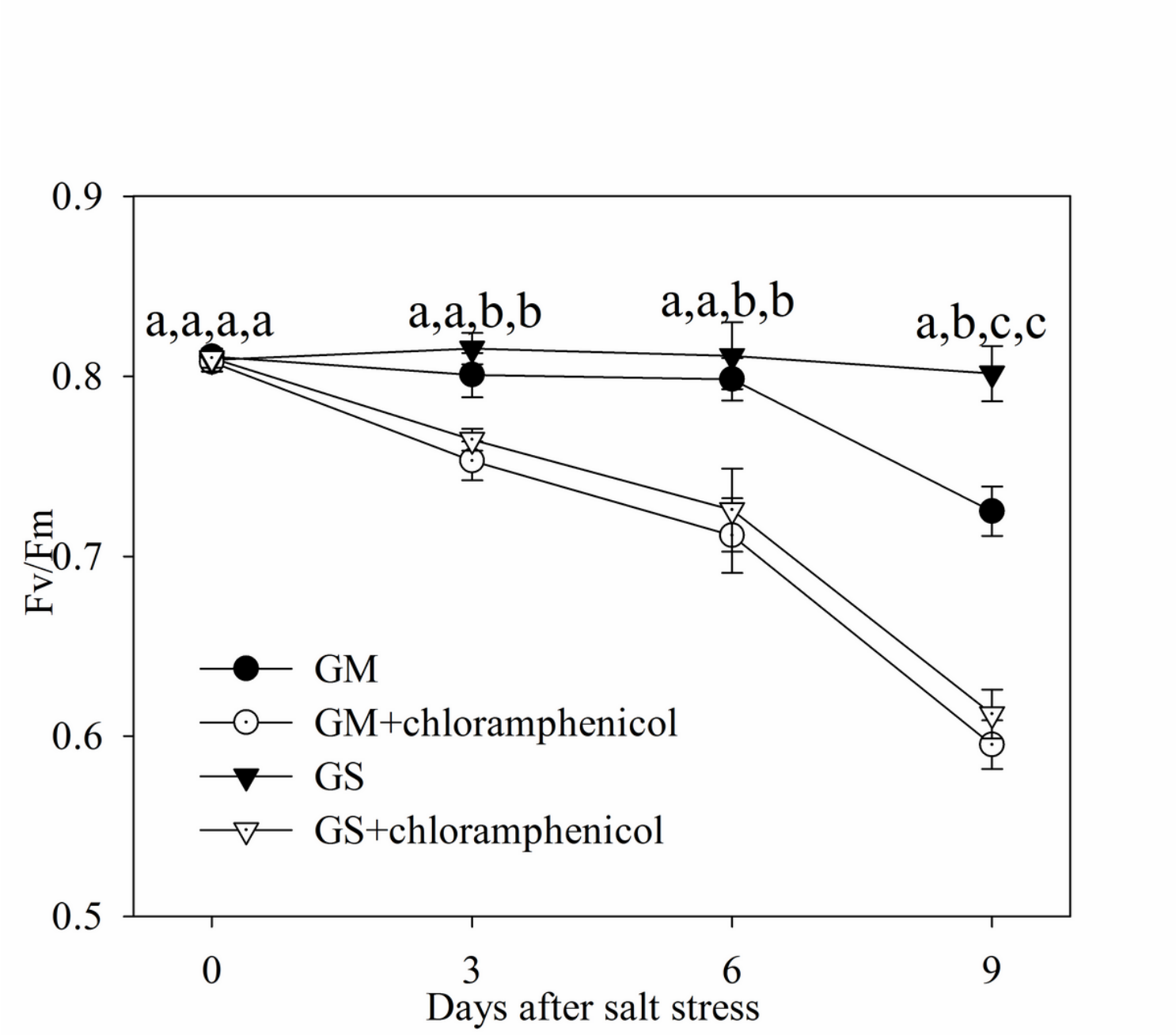

Figure 5

The maximal photochemical efficiency of PSII (Fv/Fm) in Glycine max (circles) and Glycine soja (triangles) exposed to 300 mM NaCl in the absence (closed symbols) or presence (open symbols) of chloramphenicol. For reagent treatment, leaves of Glycine max and Glycine soja were immersed in 0 or 1 mM chloramphenicol for 3h in the dark before salt stress. Data in the figure indicate the mean of five replicates (±SD). Different letters indicate significant difference among GS, GM, GS+chloramphenicol and GM+chloramphenicol at P < 0.05.

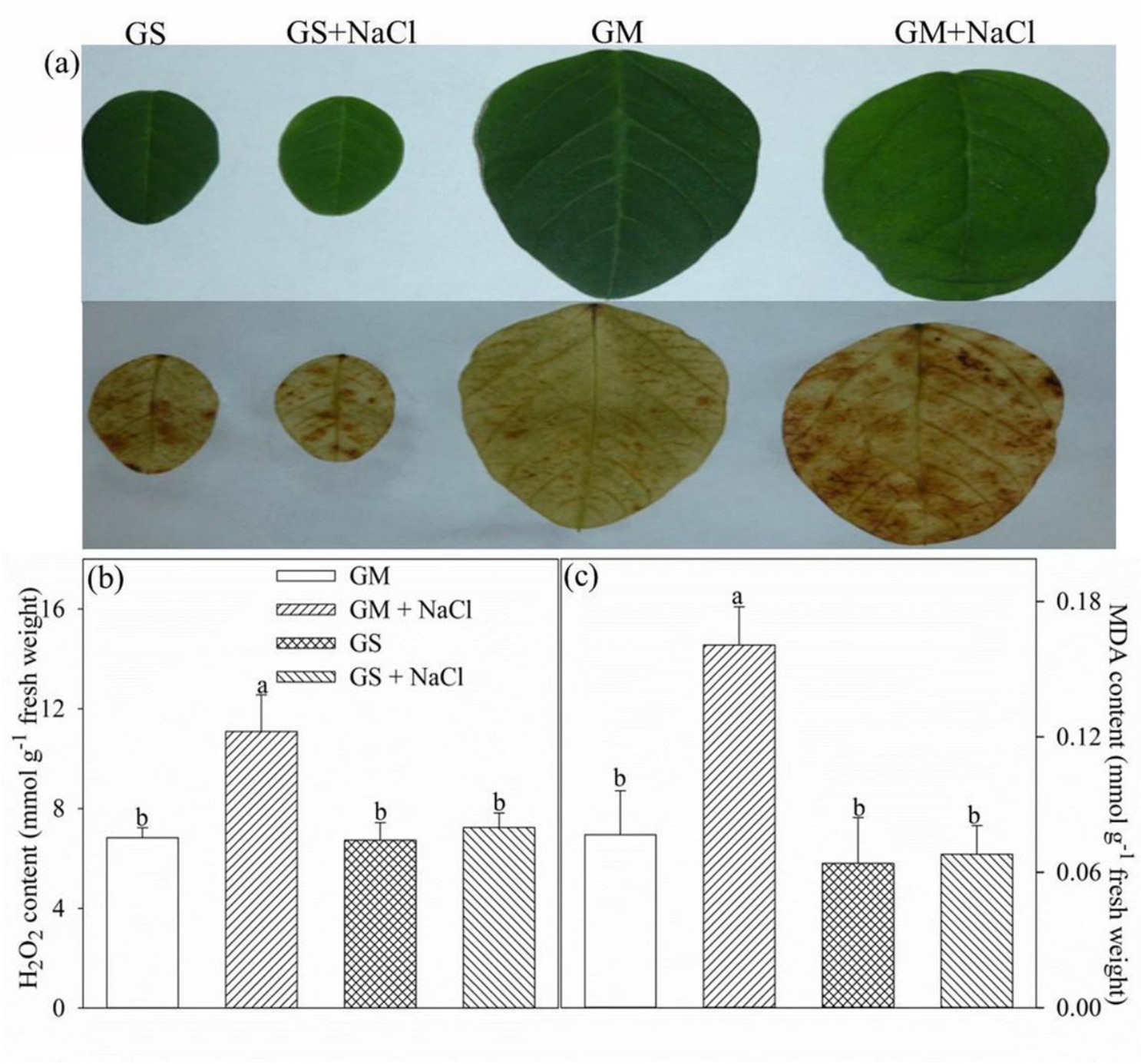

Figure 6

Histochemical detection of H2O2 (a), malondialdehyde (MDA, b) and H2O2 (c) contents in the leaves of Glycine max (GM) and Glycine soja (GS) after 9 days of salt stress with 300 mM NaCl. These symbols were also used in the following figure. Data in the figure indicate the mean of five replicates (±SD), and different letters on error bars indicate significant difference between salt treatment and control at $P < 0.05$.

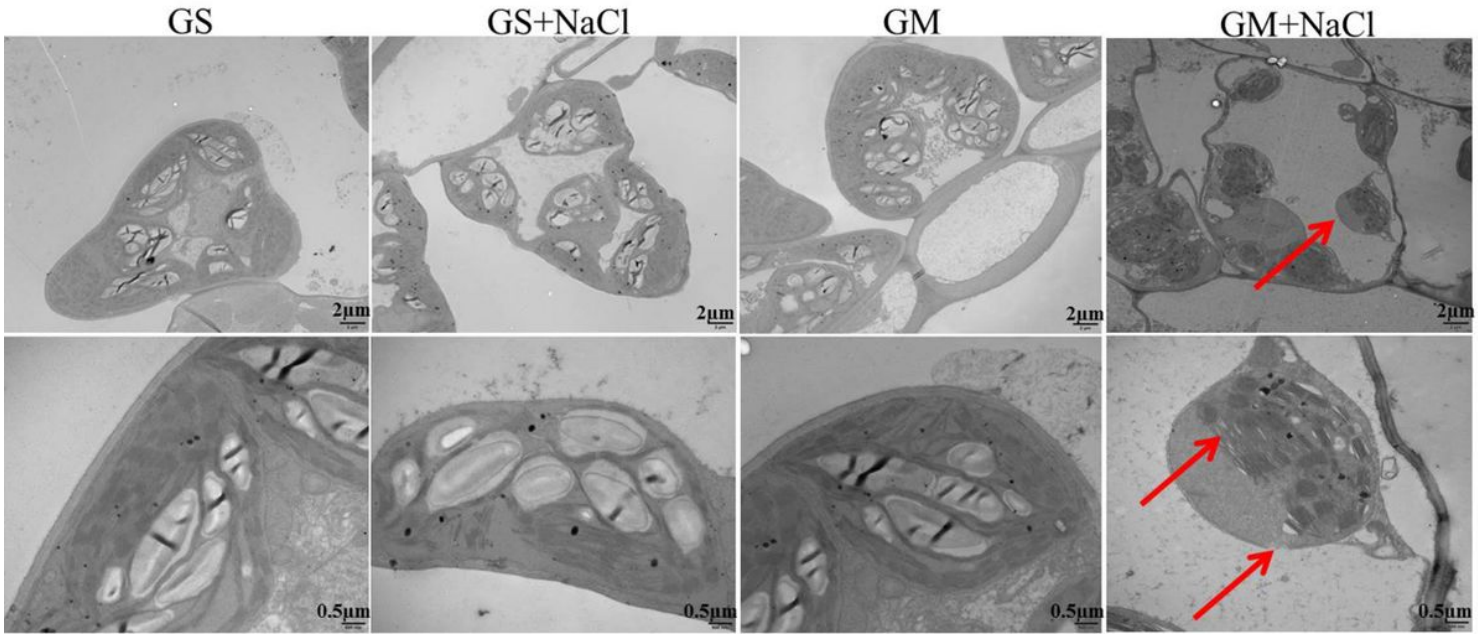

Figure 7

Ultrastructure of leaf chloroplast in Glycine soja (GS) and Glycine max (GM) after 9 days of salt stress with 300 mM NaCl. Red arrows indicated that separated chloroplast from cell wall with great reduction of starch granules, disintegrated chloroplast envelope and distended thylakoids in Glycine max upon salt stress.

Supplementary Files

This is a list of supplementary files associated with this preprint. Click to download.

- Additionalfile1FigureS1.tif
- Additionalfile1FigureS1.tif